The Use of Time Series Analysis for the Study of Respiratory Motion Artefacts in MRI/MRS: Review and Initial Results from the Use of the Lomb-Scargle Periodogram

Theodoros N. Arvanitis and Des Watson

UNIVERSITY OF

SUSSEX

AT BRIGHTON

Cognitive Science
Research Papers

The Use of Time Series Analysis for the Study of Respiratory Motion Artefacts in MRI/MRS: Review and Initial Results from the Use of the Lomb-Scargle Periodogram

Theodoros N. Arvanitis and Des Watson

School of Cognitive & Computing Sciences
University of Sussex, Falmer, Brighton, BN1 9QH, UK
Email: {theoa},{desw}@cogs.susx.ac.uk

June 25, 1997

Abstract

Various sources of systematic error exist for both Magnetic Resonance Imaging and Spectroscopy. In particular, MRI and MRS are sensitive to any type of microscopic and macroscopic motion. In this paper[1] we study the use of the Lomb-Scargle periodogram in the analysis of k-space data from motion artefacted MR images and spectra, while we provide a detailed review on the theoretical foundations of this method. We investigate the usefulness of this technique for detecting suspected periodic and quasi-periodic perturbations in MR signals, introduced by respiratory motion. Our work strongly suggests that the Lomb-Scargle periodogram can offer interesting qualitative information, relating to the effect of motion artefacts in MRI/MRS. The paper discusses the issues relating to the future use of this method for the identification and analysis of systematic errors in clinical MRI/MRS.

1   Introduction

Time series analysis is commonly used in many scientific fields, as a means of understanding and describing complex phenomena and processes. The engineering and physical sciences have long gained benefits from the various applications of time series analysis, especially in areas relating to the interpretation of experimental data. The need for this type of mathematical analysis has been further enhanced by the current technological advances in the automation of data acquisition in numerous scientific instruments [1, 19, 35, 48, 53]. In the field of biomedical magnetic resonance, time series analysis has been evaluated only recently by independent researchers, as being a useful and important tool

---

[1] Much of this paper was adapted from the first author's 1994 DPhil thesis [4] and some recent published work from both authors [5, 9].

for the understanding of the basic MR physical processes and the analysis of interesting research problems [31, 58].

In general, we can identify two main groups of time series analysis techniques: (a) The *time domain* and (b) the *frequency domain* analysis techniques. The time domain techniques have been investigated extensively by several researchers and characterized as favourable towards the analysis of random processes [16, 26, 45, 46, 47]. On the other hand, frequency domain techniques have been found mostly suitable for the investigation of the opposite to the random processes, the so-called deterministic processes. Additionally, frequency domain analysis has always proven to have advantages for periodic phenomena [12, 15, 36].

In this paper, we examine the issues relating to the problem of respiratory motion artefacts in biomedical magnetic resonance imaging and spectroscopy, through the use of time series analysis on MR artefacted data. In particular, we introduce the use of the **Lomb-Scargle periodogram** for the analysis of k-space data, and investigate its appearance and properties when applied to MR images and spectra that have been "contaminated" by motion artefacts. In the first part of this paper, we provide the reader with the appropriate theoretical background and discuss our motivation for using this frequency domain technique as a tool for detecting suspected periodic and quasi-periodic perturbations in MR signals. In the subsequent parts, we provide some representative examples from both simulated and experimental image data, with the intention to draw conclusions on the advantages and disadvantages of the method. Furthermore, we investigate the potential use of this unconventional power spectral estimation technique for the case of MR spectroscopy.

2   Theory of Periodogram Analysis

Before we describe the Lomb-Scargle method and explain its statistical properties, we review the theoretical basis of power spectral estimation by periodogram analysis. We relate our discussion to signal detection theory (section 2.1). The solution to the problem of periodic signal detection in the presence of noise, as conveniently described by this theory, is the main motivation for the definition of the Lomb-Scargle periodogram. Furthermore, the modelling of signal and noise in the signal detection theory is found to be the most suitable for the description of the ghosting and blurring effects introduced to MR images by motion.

In section 2.2, we provide the classical definition of the periodogram and then present the theoretical derivation of the Lomb-Scargle periodogram (see section 2.3). Immediately after follows a discussion on the statistical properties of the Lomb-Scargle method (see sections 2.4 and 2.5). We use this knowledge to observe and explain the data in the experimental part of the paper. Finally, we elaborate on the application of the Lomb-Scargle periodogram for the case of MR data and assess its advantages and disadvantages in comparison with the classical approach.

2.1   Power Spectrum Estimation and Signal Detection

One of the most popular themes in time-series analysis is the estimation of the power spectrum of a measured signal. Power spectrum analysis has been used

in many scientific fields, mainly towards the solution of the signal detection problem [27, 29, 32, 45, 55].

The signal detection problem, as described in various signal and image processing textbooks [24, 45, 51, 55], can be formulated as follows. Suppose that a physical variable H is measured at a set of times t_i[2]. This measurement results in a time-series data, here denoted as $\{H(t_i), i = 1, 2, 3, ..., N\}$, which is called the observed digitized signal. This data set is assumed to be the sum of a pure signal and random observational errors. Consequently, the times series data can be represented by the following expression [24]:

$$H_i = H(t_i) = S(t_i) + N(t_i) \tag{1}$$

where $S(t_i)$ is the pure signal and $N(t_i)$ represents the observational errors during the measurement of the signal. Because of the additive relationship between the pure (or original) signal and the parameter $N(t_i)$ in equation (1), the latter is often called the **noise**. For many applications of the signal detection theory, the noise is assumed to be random [24, 38, 40, 56], which means that the observational errors at distinct times are statistically independent. Furthermore, in a significant number of cases, the noise is usually assumed to have a normal distribution with zero mean and constant variance σ_o^2, hence the term "Gaussian noise" [24, 40].

In many scientific measurement applications, noise can badly corrupt the observed signal. The main motivation behind the signal detection theory is the solution to this problem, that is to establish the existence of a signal in the presence of noise. In addition to this, researchers used the framework provided by the theory to investigate other important problems. For example, one might want to identify the presence of a periodicity in a "noisy" signal or estimate the harmonic content of a periodic signal (either by the detecting the principal signal harmonic or its multiple). Other interesting problems are the frequency or period calculation of a particular signal harmonic and the removal of random noise from the observed signal. In the context of the Lomb-Scargle formulation, we will use the framework of signal detection theory for the identification of any periodic content in a "noisy" signal that has been *unevenly* sampled.

The problem of respiratory motion artefacts can be reformulated under the philosophy of signal detection theory. We can characterize the ghost-like respiratory motion artefacts as being a type of systematic noise. The systematic error introduced by motion is a replicated and unrealistic MR signal intensity added to the pure MR signal. For example, the idea of the ghost mask, introduced by Xiang and Henkelman [60], shows this additive relationship.

Based on the above argument, we formulate the signal detection problem for this study. Thus, if we set $G(t_i)$ to represent the systematic error introduced by the breathing artefact, then according to equation (1), the observed digitized MR signal (here denoted as S_i') can be described as a time series data set by the following expression[3]:

---

[2] The set of observation times $\{t_i\}$ is called the *sampling*. For the purposes of our description, we use the term *even sampling* when $\Delta t_i = t_{i+1} - t_i = c$, where c is constant. When this condition is not true for the different values of observation times we use the term *uneven sampling*.

[3] For simplicity, equation (2) assumes that only the presence of motion artefacts and random noise contaminates the pure MR signal. Any other sources of systematic error are considered to be insignificant for the purposes of this study, and are therefore ignored.

$$S_i' = S(t_i)' = S(t_i) + G(t_i) + N(t_i) \tag{2}$$

Therefore, in the context of signal detection theory, equation (2) constitutes the basis for the following study. MR images and spectra are described as time series data sets and we aim to detect any harmonic content in the MR signal that corresponds to the effects of motion. Thus, the aim of this study is to investigate the influence of $G(t_i)$ signal – which corresponds to the effect of motion artefacts – on the periodogram of $S(t_i)$ (i.e. the observed MR signal).

As mentioned before, power spectrum estimation is frequently used for the solution of the signal detection problem. Several interesting and successful approaches have been developed for the estimation of the power spectrum [20], mainly by using the Fast Fourier Transform (FFT) [13, 23, 43, 52]. One of the most popular power spectrum estimation techniques is accomplished by means of the periodogram. In the literature, one can find considerable research that has been undertaken on the so-called periodogram analysis [21, 25, 28, 30, 39, 41, 42]. This approach makes a good use of the periodic nature of the signal and aims to give a complete description and understanding of the periodicity. In the following section we will describe the classical formulation for the periodogram.

2.2 The Classical Periodogram

We can define the discrete Fourier transform of an evenly sampled data set, $\{g(t_i), i = 1, 2, 3, ..., N\}$, as follows [14]:

$$\Im\{g(t_i)\} = G(f) = \sum_{i=0}^{N-1} g(t_i)e^{-j\,2\pi f t_i/N} \tag{3}$$

or by substituting the frequency f by the angular frequency ω, where $\omega = 2\pi f$, then equation (3) becomes:

$$\Im\{g(t_i)\} = G(\omega) = \sum_{i=0}^{N-1} g(t_i)e^{-j\,\omega t_i/N} \tag{4}$$

Conventionally the classical periodogram is defined [13, 21, 23, 43, 52] as:

$$
\begin{aligned}
P(\omega) &= \frac{1}{N}|G(\omega)|^2 \\
&= \frac{1}{N}\left|\sum_{i=0}^{N-1} g(t_i)e^{-j\,\omega t_i/N}\right|^2 \\
&= \frac{1}{N}\left\{\left[\sum_{i=0}^{N-1} g(t_i)\cos\omega t_i/N\right]^2 + \left[\sum_{i=0}^{N-1} g(t_i)\sin\omega t_i/N\right]^2\right\}
\end{aligned}
\tag{5}
$$

The classic periodogram equation (5) can be evaluated for any value of angular frequency and the presence of a periodic signal is indicated by a large value of P at one particular value of ω. This usually appears as a distinct narrow peak in the periodogram's power spectrum estimate. Although the above expression

4

can be evaluated at any frequency, it is traditionally evaluated only at a special set of $N' = N/2$ evenly spaced frequencies [21, 23, 43, 52]. However, this particular definition of the classical periodogram has two important problems:

1. The classical periodogram presents several statistical difficulties. This, in simple words, means that the function $P(\omega)$ of the periodogram is very noisy [52, 57] and several techniques for further processing and optimization are required.

2. There exists the major problem of spectral leakage [20, 44, 51]. This means that for any periodic signal at a specific frequency, the power in the periodogram does not appear only at that frequency, but also "leaks" into other frequencies (a typical example of spectral leakage is the well-known phenomenon of aliasing [14, 17, 18]). In the literature there exists a significant amount of work describing the problem of spectral leakage and the related techniques used to overcome the "leakage" effects. [10, 33, 59].

Furthermore, this definition does not cope with data sets that are not evenly sampled. For this reason, Scargle [54] derived a new definition of the periodogram, which will be described in the following section. Because of some interesting similarities to a power spectrum estimation technique that Lomb formulated on 1976, we will call this periodogram the Lomb-Scargle periodogram.

2.3   The Lomb-Scargle Periodogram

As already mentioned in the previous section, the classical periodogram and its statistical distribution have been successfully investigated for the case of evenly sampled data sets. Usually, the distribution of the power spectrum has an exponential shape. This has been shown for the case in which the evenly sampled data set $g(t_i)$ is pure Gaussian noise [30]. A similar result has been derived for the more general case of data sets with uneven sampling. Thus, a modified version of the classical periodogram has been defined by Jeffrey Scargle – an eminent researcher at the NASA Ames Research Center – to cope with the case of unevenly sampled data sets [54]. The power spectrum estimate provided by the modified periodogram has the same exponential distribution as in the even-sampling case [11, 34, 49, 50, 54]:

$$
P(\omega) = \frac{1}{2} \left\{ \frac{\left[\sum_{i=0}^{N-1} g(t_i) \cos \omega (t_i - \tau) \right]^2}{\sum_{i=0}^{N-1} \cos^2 \omega (t_i - \tau)} + \frac{\left[\sum_{i=0}^{N-1} g(t_i) \sin \omega (t_i - \tau) \right]^2}{\sum_{i=0}^{N-1} \sin^2 \omega (t_i - \tau)} \right\} \quad (6)
$$

where $i = 0, 1, 2, ..., N-1$ is the index of the unevenly spaced observation times. The term τ can be defined by the following expression:

$$
\tan 2\omega\tau = \frac{\left(\sum_{i=0}^{N-1} \sin \omega t_i \right)}{\left(\sum_{i=0}^{N-1} \cos \omega t_i \right)} \quad (7)
$$

This new form of the periodogram, even though significantly altered from the classical periodogram definition of equation (5), gives values very similar to the classical formulation, as already demonstrated by Scargle [11, 54].

Scargle argues [54] that the modified form of the periodogram can replace the classical definition, for the following reasons:

1. The redefined periodogram has a simple statistical behaviour, even better than that of the classical periodogram definition for the even-sampling case [54].

2. The use of the time constant τ gives to the periodogram a time-translation invariance. In other words, the constant τ makes P completely independent of any time shift of time t_i [50, 54].

3. Finally, this offset of time makes the present method of the periodogram estimation equivalent to the reduction of the sum of squares in least squares fitting of sine waves of the data, a method mainly investigated by Lomb [39]. Hence the equation (6) of the periodogram is almost identical to the equation of the estimation of the harmonic content of a data set, at a given frequency ω, by linear least-squares fitting to the model:

$$g(t) = A \cos \omega t + B \sin \omega t \qquad (8)$$

From the above, it is obvious why this method can be more successful than the other FFT power estimation methods, especially for the case of uneven sampling, since it weights the data on a "per point" basis instead of on a "per time interval" basis [50].

By observing equations (6) and (7), the computation of the Lomb-Scargle periodogram seems complex. However, a concrete and clear algorithm has been constructed for this calculation. We use a very fast and powerful algorithm for our periodogram analysis, which is based on the work of Press and Rybicki [49, 50].

2.4 The Statistical Behaviour of the Lomb-Scargle Periodogram

The usefulness of periodogram analysis can be seen in the effectiveness of the method to evaluate and quantify the appearance of the power spectrum produced. Often, power spectra have a complicated appearance. In particular, when the data sets under analysis are noisy, then the power spectra have a similar noisy appearance. For this reason, it is important to find a quantitative way to identify whether any large spectral peak occurring in the periodogram represents pure signal, random noise or spurious signal corresponding to systematic error.

A way towards the evaluation of the significance of spectral peaks in the Lomb-Scargle periodogram is by examining the probability of an observed feature to have arisen from a random (noisy) fluctuation.

Scargle presented a simple and robust statistical approach to evaluate the significance of spectral peaks in the periodogram [54]. He took a null hypothesis in which the data values are assumed to be independent random Gaussian values (i.e. pure Gaussian noise), and then tested its viability.

In order to test the viability of the null hypothesis, Scargle used the following methodology. First, he proved that by normalizing the modified periodogram by a factor of σ^2, at any particular angular frequency ω and in the case of his

null hypothesis, the power spectrum $P(\omega)$ (and in effect the power at a given frequency) has an exponential distribution with zero mean and noise variance equal to unity [11, 54].

This can be seen in the following formulation. If we let $Z = P(\omega)$ then the probability distribution (here denoted as p_Z) is given by:

$$p_Z(z)dz = Pr(z < Z < z + dz) = \exp(-z)dz \qquad (9)$$

where Pr denotes the probability.

Also, the cumulative distribution F_z can be calculated easily:

$$F_Z(z) = Pr\{Z < z\} = \int_0^z p_Z(z')dz' = 1 - \exp(-z). \qquad (10)$$

Before examining further the statistical behaviour of the periodogram, we should mention that the normalization factor σ^2 is the total variance of the data. Horne and Baliunas have shown [34] that only if the total variance of the data is used as the normalization factor for the Lomb-Scargle periodogram, then the periodogram will have the expected exponential probability distribution mentioned above. With this normalization factor, the equation (6) that describes the Lomb-Scargle periodogram becomes:

$$P(\omega) = \frac{1}{2\sigma^2} \left\{ \frac{\left[\sum_{i=0}^{N-1} g(t_i) \cos \omega (t_i - \tau)\right]^2}{\sum_{i=0}^{N-1} \cos^2 \omega (t_i - \tau)} + \frac{\left[\sum_{i=0}^{N-1} g(t_i) \sin \omega (t_i - \tau)\right]^2}{\sum_{i=0}^{N-1} \sin^2 \omega (t_i - \tau)} \right\}$$
$$(11)$$

Now, one can see from equations (9) and (10) that one useful quantity is the $Pr\{Z > z\} = \exp(-z)$, which gives the statistical significance of any large observed spectral power peak at the corresponding preselected frequency. Thus, as the power level becomes larger, there is less chance of an observed power level corresponding to random fluctuations (noise).

Scargle showed that if we consider the largest value $Z = \max_M P(\omega_M)$ in the spectrum over a set of independent M frequencies [11, 54], then the probability of this value being the largest significant is given by:

$$Pr\{Z > z\} = 1 - F_Z(z) = 1 - [1 - \exp(-z)]^M \qquad (12)$$

This measure can be significant even if a pure noisy data set is investigated. It has been claimed that, if many independent frequencies are inspected for a spectral peak, then one expects to find a large power peak even if no signal is present.

The number of independent frequencies M to be observed can be calculated in relation to the total number of time points N. This number has been derived by Horn and Baliunas [34] and is given by the following empirical formula:

$$M = -6.362 + 1.193N + 0.00098N^2 \qquad (13)$$

We can now test the viability of the null hypothesis in terms of the false alarm probability.

2.5 The False Alarm Probability

It is desired to find a power level, z_o, such that if the power exceeds this level, the error in declaring a detected peak as being significant will be very small. The probability of this fault, p_o, is called the false alarm probability of the null hypothesis and it can be fixed to be a small number, so that the detected peaks have high significance. The above mentioned threshold power level can be derived by the distribution in equation (12) and is given by the following expression:

$$z_o = -\ln[1 - (1 - p_o)^{1/M}] \tag{14}$$

where M are the independent observed frequencies used in the calculation of the normalized Lomb-Scargle periodogram.

For small p_o, equation (14) becomes

$$z_o \approx \ln(M/p_o) \tag{15}$$

For example, if we take $p_o = 0.01$, which means we have a 99% significance level, then z_o is given by the following expression:

$$z_o \approx 4.6 + \ln(M) \tag{16}$$

We will use expressions (15) and (16) to identify the significance levels of the experimental results presented in the second part of this chapter.

3 Time-Series Analysis and Respiratory Motion Artefacts in MR: The Reasoning Behind the Use of the Lomb-Scargle Periodogram

As we have argued in a previously published study [6], the effect of motion in spectroscopic Chemical Shift Imaging (CSI) is manifested in the appearance of spectra as signal re-distribution and as an overall increase in the background noise level. Our initial experience in both cardiac and hepatic ^{31}P MRS studies on volunteers showed small (5–10%) but consistent improvements in the overall signal-to-noise ratio (SNR) of the spectra when the Respiratory Ordered Phase Encoding (ROPE) method was used. On the spectra, these changes appeared to be visually more significant in the level and the character of the noise, rather than in the signal level itself. These visual observations have suggested the importance of further understanding the source and appearance of motion artefacts in spectroscopic CSI investigations. Thus, we used the autocorrelation function, a typical Fourier transform time-series analysis approach, to identify the character of random and systematic noise (motion artefacts) upon both 2D-FT imaging and 1D CSI spectroscopic data. The selection of this technique was based on the opinion that the autocorrelation function of time series data completely specifies the first- and second-order noise statistics of Gaussian processes [24]. We applied both the one-dimensional and the two-dimensional versions of the autocorrelation function in data from phantom MRI and MRS studies. The result of this time series analysis investigation showed high order correlations arising from motion artefact effects. Furthermore, when comparing

the three cases of image acquisitions of a moving phantom, a static phantom and a moving ROPE'd phantom, we identified significant differences in their MR data autocorrelation functions.

Although these results were found promising at the time, all observations were purely qualitative. There was still a need to quantify these results, so that we could have precise information about the correlation of motion with any time series analysis of the MR data. In order to satisfy this need we investigated time series analysis techniques even further. The technique we adopted was the power spectrum estimation of the MR data by means of periodogram analysis.

In the past, Weisskoff et al. had applied the classical Fourier periodogram analysis on functionally-weighted MR data [58], where they produced 128 point periodograms. These periodograms were produced by using power spectrum images of the MR data and by applying on them the traditional "overlap-add" method, that is often used for several Fourier frequency-domain techniques (e.g. convolution, correlation, etc.) [50]. In their case, the problem of spectral leakage was dealt with by the application of a 4-term Kaiser-Bessel window function. These periodograms assumed that the data was evenly spaced. For the work of Weisskoff et al., this assumption was appropriate due to the fact that the MR data was very rapidly acquired by single-shot Echo-Planar Imaging (EPI). However, the use of this traditional type of periodogram analysis for investigating motion artefacts in 2D-FT imaging and 1D CSI spectroscopy, is not very effective. This is explained by the fact that in these cases, the collected MR data set is composed of several complex FID signals, where there exists a time delay TR between the subsequent acquisitions of these signals. Thus, if we treat the MR data set as a single time series, we can assume that this time series data set is unevenly sampled. It is therefore essential that we introduce the use of the Lomb-Scargle periodogram for the study of respiratory motion artefacted MR data.

4 Methodology

In this section, we present the implementation of the normalized Lomb-Scargle periodogram for the analysis of both simulated and experimental MR data. The algorithm used for the calculation of the periodogram was based on a computational approach, which Press and Rybicki had presented in 1989 [49]. We discuss particular aspects of this approach and the way the Press and Rybicki algorithm is implemented for our study. In addition, we elaborate on the methodology used for the treatment and analysis of simulated image data, experimental image data and experimental spectroscopic data.

4.1 The Lomb-Scargle Periodogram Algorithm

The implementation of the Lomb-Scargle method is computationally straightforward. One can input a set of data points and their respective observation times in equation (11) and output the power spectral estimation of this data for a set of angular frequencies. However, the Lomb-Scargle method, which has been frequently used in the analysis of astrometric data, has always been viewed as a "slow" computational method for large data sets. As it can be seen from equation (11), multiple calls of trigonometric functions should be com-

bined for each data point. As suggested by Press and Rybicki [49, 50], these computational calls might require operations of order $\mathcal{O}(N^2)$ to analyze N data points against their observation times. In order to cope with this, Press and Rybicki suggest a fast algorithm for the Lomb-Scargle method, which reduces the computation to an order of $\mathcal{O}(N)$.

This algorithm uses Fast Fourier Transforms (FFTs) [17, 18, 43, 14] to accelerate the computation of the trigonometric functions in equation (11). This is accomplished by a technique called *extirpolation*, which is equivalent to inverse interpolation[4]. This fast algorithm makes feasible the application of the Lomb-Scargle periodogram to time series data sets with size up to 10^6 points.

At this stage we should clarify a few practical points concerning the implementation of this algorithm in our study. Horn and Baliunas proposed an empirical formula (see equation 13) in order to calculate the minimum number of independent frequencies over which the periodogram should be optimally evaluated. In the fast Lomb-Scargle periodogram algorithm, the number of independent frequencies M is proportional to the number of data points and to two input factors: an *oversampling factor* and a *highest frequency indicator factor* [50]. The oversampling factor, here denoted as *ofac*, represents how finely one wishes to oversample the independent frequencies, so that more significant power spectral peaks can be observed. The highest frequency indicator factor, here denoted as *hifac*, is the ratio of the highest frequency over which we observe the periodogram and the periodogram's "experimental Nyquist frequency"[5]. The formula that provides the number of independent frequencies M is

$$M = \frac{ofac \times hifac}{2} N \qquad (17)$$

During our study we have set *ofac* = 4 and *hifac* = 1, always observing the periodogram over a number of frequencies, twice as many as the input data points. It is important to clarify that the output of the implemented program returns an increasing sequence of frequencies corresponding to the different values of the power spectrum. These frequencies are not angular frequencies, as one would expect by the definition of the Lomb-Scargle periodogram in equation (11).

We used the C programming language [37] to implement the Press and Rybicki algorithm.

4.2 Simulated and Experimental Data

We acquired both simulated and experimental data to be processed by the normalized Lomb-Scargle periodogram.

In order to understand the output of the periodogram under well-controlled conditions, we used a series of simulated data sets provided by our 2D-FT MR imaging simulator [2, 8, 3]. A point-like object – a homogeneous disk (5 pixels in

---

[4] In the original paper by Press and Rybicki [49] the term "extirpolation" is thoroughly explained, together with the details of their implementation. Such a discussion at this point would be out of the scope of this paper.

[5] We use the term "experimental Nyquist frequency" to describe the frequency value which one would obtain if the data points were evenly spaced over the same time span. In our case, it is obvious that this value is different from the MR signal's Nyquist frequency of sampling.

diameter) – was used for the creation of k-space data. We created image data corresponding to image acquisitions for both stationary and moving objects. Furthermore, we also acquired simulated data corresponding to images corrected by the ROPE method. All k-space matrices that we constructed were of size 64×64. We reduced the 2D matrices to single 1D arrays of 4096 data points, thus treating the FID signals in the data as a single time series signal, unevenly sampled. These data points together with the corresponding observation times[6] constituted the input data for the normalized Lomb-Scargle periodogram. In this case we evaluated the periodogram at 8,192 independent frequencies. No prior processing of the data was performed, and the periodogram was evaluated for the magnitude of the FID signals.

As well as using simulated data, we performed periodogram analysis on actual experimental MRI and MRS data sets. All experimental work was carried out on a Picker prototype MRI/MRS system, operating at a field of 1.5 Tesla, at the Robert Steiner MRI Unit, Hammersmith Hospital, London.

The subject of the study was a simple phantom [7, 22], constructed with non-magnetic materials (Perspex and plastic). This phantom consisted of a cylinder (height 10 cm, diameter 5 cm), filled with a $CuSO_4$ solution. A mechanical device was designed to provide a variable vertical displacement of the cylinder. The phantom was mechanically coupled by the use of a long shaft to a DC step electric motor positioned 6 meters away from the centre of the bore of the main magnet. The electric motor provided the driving mechanism that applied periodic displacement on the phantom. The amplitude and the period of the displacement could be varied in order to model the effects of human respiratory motion. Figures 1 and 2 show the profile and semi-lateral photographic views of the phantom.

We acquired data by using both 2D-FT imaging and 1D spectroscopic CSI methods. Images and spectra were obtained for the cases of static and periodically moving phantoms. Furthermore, ROPE acquisitions of the moving phantom were implemented in both 2D-FT imaging and 1D CSI spectroscopy. Again, the resulting k-space MR data was treated as a single time series. In the case of image data, the size of the k-space matrices was 256×128, thus the Lomb-Scargle periodogram was evaluated at 65,536 independent frequencies. In the case of spectroscopic data, k-space matrices were of size 128×64, and thus the Lomb-Scargle periodogram was evaluated at 16,384 independent frequencies. For all experimental data, we performed processing prior to the periodogram analysis. As the data originated from VAX workstations and analysis was performed on Sun SPARC workstations, data had to be byte-swapped and floating point formats modified where appropriate. Following this operation, we obtained the values of any DC offsets from both the real and imaginary parts of the data. To achieve more accurate results, we have calculated the DC offsets for each line, although one can obtain a less accurate global DC value from the MR system. The DC offset was calculated by averaging the 10 last data values (either real or imaginary values) on each line. The Lomb-Scargle periodogram was evaluated for both real and imaginary parts of the k-space imaging and spectroscopic data.

---

[6] The observation times were given in the form of an one-dimensional array of data and were not equally spaced, as between consecutive FID's there exists a significant time gap, due to the repetition time (TR).
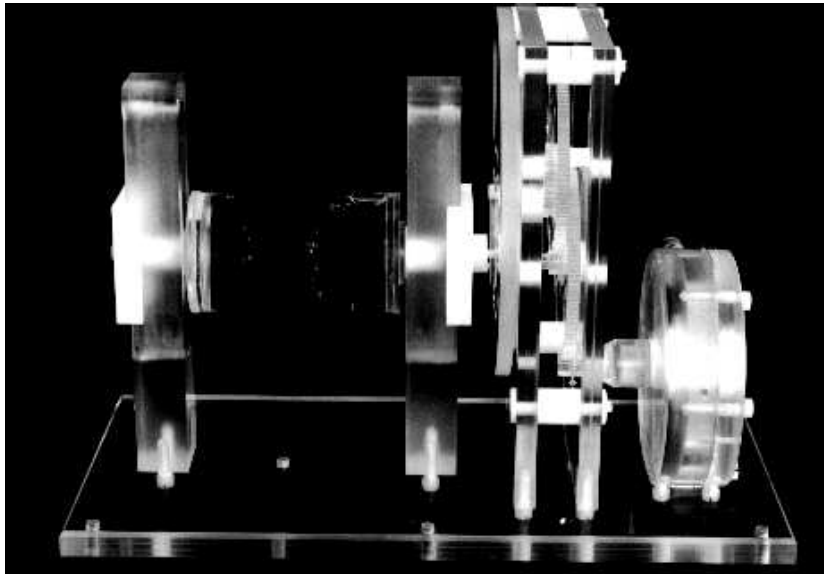
Figure 1: Profile view of the experimental phantom

In the following section we observe representative results from our simulated and experimental work.

5 Results

5.1 Periodogram Analysis on Simulated Image Data

We collected a set of representative periodogram results of 2D-FT imaging data, originating from a simulated point-like object. In this set of experiments, the object was moving with a motion amplitude set at 15 pixels. For each row of the data matrices, data points were sampled every 0.04 msec of simulated time at 500 msec TR intervals. These imaging parameters were kept constant for all experiments. The only factor that was altered was the period of the movement of the object. For four different frequencies of motion, we compared the appearance of the periodogram using data from the moving object and data that was controlled by our implementation of the Respiratory Ordered Phase Encoding (ROPE) method. These periodograms were further compared to the appearance of the Lomb-Scargle periodogram of image data of a static object.

As mentioned in the previous section, the periodogram was evaluated at 8,192 independent frequencies, ranging from 0 kHz to the periodogram's experimental Nyquist frequency, which for this case was 64 kHz[7]. For convenience, we compared all results by studying the periodogram in a window around the maximum observed peak.

---

[7] The total simulated time of the imaging experiment was 32 sec. One can calculate the periodogram's experimental Nyquist frequency by dividing the total number of points in the data set by twice the total imaging time.
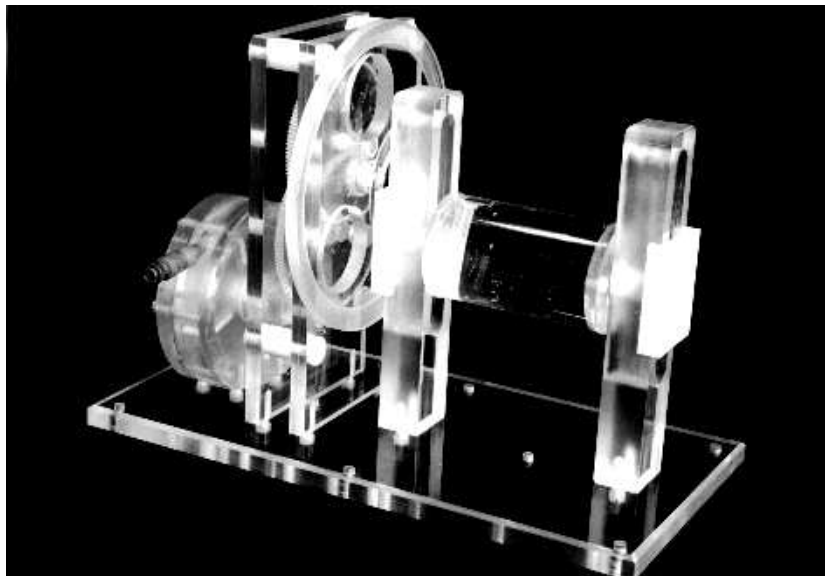
Figure 2: Semi-lateral view of the experimental phantom

The significance of the power spectrum levels has been evaluated by using the false alarm probability condition, as given by equation (14). For these experiments, we have set a significance level of 80%, which determines a detection threshold $z_o = 10.62 \text{cycles/mm}^2$. So, below this threshold any observed peak is assumed to be noise. Table 1 summarizes the observations made from the different data sets.

The above table gives the value of the maximum peak power and its corresponding observed frequency, while it identifies the range of frequencies [around $P(f_{\max})$], over which the observed power spectrum values are significant. At first glance, one can see that for the moving object, at various frequencies of motion, the maximum power level changes dramatically if compared to the maximum power level of a static object. Also, one can identify a shift in the frequency at which $P(f_{\max})$ is observed. As the frequency of motion increases, this shift tens to become larger. The ROPE'd data shows that this motion artefact suppression method tries to establish both the original static power spectrum levels and their corresponding observed frequencies.

Looking at the appearance of the power spectral estimation plots for the above data sets, in figures 3, 4, 5 and 6, we can identify the qualitative differences between the static and the moving objects, while it is very difficult to make any quantitative comparisons. At this stage, we can simply observe minor visual differences between the static and moving power spectra. Only in the case of figure 3.C, one can identify additional significant harmonics on the side of the maximum peak. However, the appearance of the ROPE'd data is dramatically different. We can see that although ROPE tries to re-instate power spectrum levels close to those of the static object, in some instances it creates additional harmonics to the periodogram. This is obvious in figures 4.B and 5.B, where significant levels of periodic power peaks can be identified. Again, here we meet

13

Status	$P(f_{\mathrm{max}})$ (cycles/mm^2)	Observed Freq. (kHz)	Freq. Range (kHz)
static	206.03	26.04	$25.82 - 26.18$
moving (no ROPE) $- 0.10$ Hz	211.07	28.04	$27.87 - 28.05$
moving (ROPE) $- 0.10$ Hz	169.40	23.83	$23.75 - 24.01$
moving (no ROPE) $- 0.25$ Hz	260.75	30.04	$29.87 - 30.13$
moving (ROPE) $- 0.25$ Hz	149.94	25.91	$25.75 - 25.98$
moving (no ROPE) $- 0.35$ Hz	188.13	34.04	$33.76 - 34.25$
moving (ROPE) $- 0.35$ Hz	168.50	11.98	$11.62 - 12.10$
moving (no ROPE) $- 0.45$ Hz	296.75	40.04	$39.87 - 40.13$
moving (ROPE) $- 0.45$ Hz	236.06	11.90	$11.81 - 12.06$

Table 1: Maximum observed power spectrum level for simulated data. For this data a point-like object has been used (5 pixels in diameter), moving with a motion amplitude set to 15 pixels. Four different experiments were set up, where the object had four different motion periods, corresponding to frequencies of 0.10 Hz, 0.25 Hz, 0.35 Hz and 0.45 Hz.

the quantitative observations made in table 1.

The symmetry seen in the periodogram corresponds to the spin-echo character of the simulated MR signal.

We will discuss these results further in section 6.1.

5.2   Periodogram Analysis on Experimental Image Data

This section presents examples of our Lomb-Scargle periodogram analysis experiments on the k-space data of a 2D-FT imaging phantom study, called *mot1*. We have chosen this study for demonstration, as it is an example of a typical spin-echo imaging acquisition. For the *mot1* data set, signals have been acquired by using a 15cm diameter surface ^{31}P/^{1}H coil.

The size of the k-space 2D matrices examined was 256×128. To apply the Lomb-Scargle periodogram on the acquired MR data, we formulated a single time series from the k-space data matrix points. As explained above, this single time series is assumed to be unevenly sampled. As a consequence, the input time series data set for our periodogram analysis consisted of 32,768 k-space data points. For each point we assigned a corresponding observation time variable. The sampling of the MR signal was performed every 0.04 msec, while the TR was 1000 msec. The total experiment time was 128 seconds.

The Lomb-Scargle periodogram has been evaluated at 65,536 independent frequencies, ranging from 0 kHz to the periodogram's experimental Nyquist frequency, which for this case was 128 kHz. The Lomb-Scargle periodogram of the different k-space data sets was investigated separately for the real and imaginary parts of the data.

The significance of the power spectrum levels has been evaluated by using the false alarm probability condition that Scargle introduced (see equations 14, 15, and 16). For these experiments, we have set a significance level of 95%, which determines a detection threshold $z_o = 14.08$cycles/mm^2. So, below this threshold any observed peak is assumed to be pure noise.
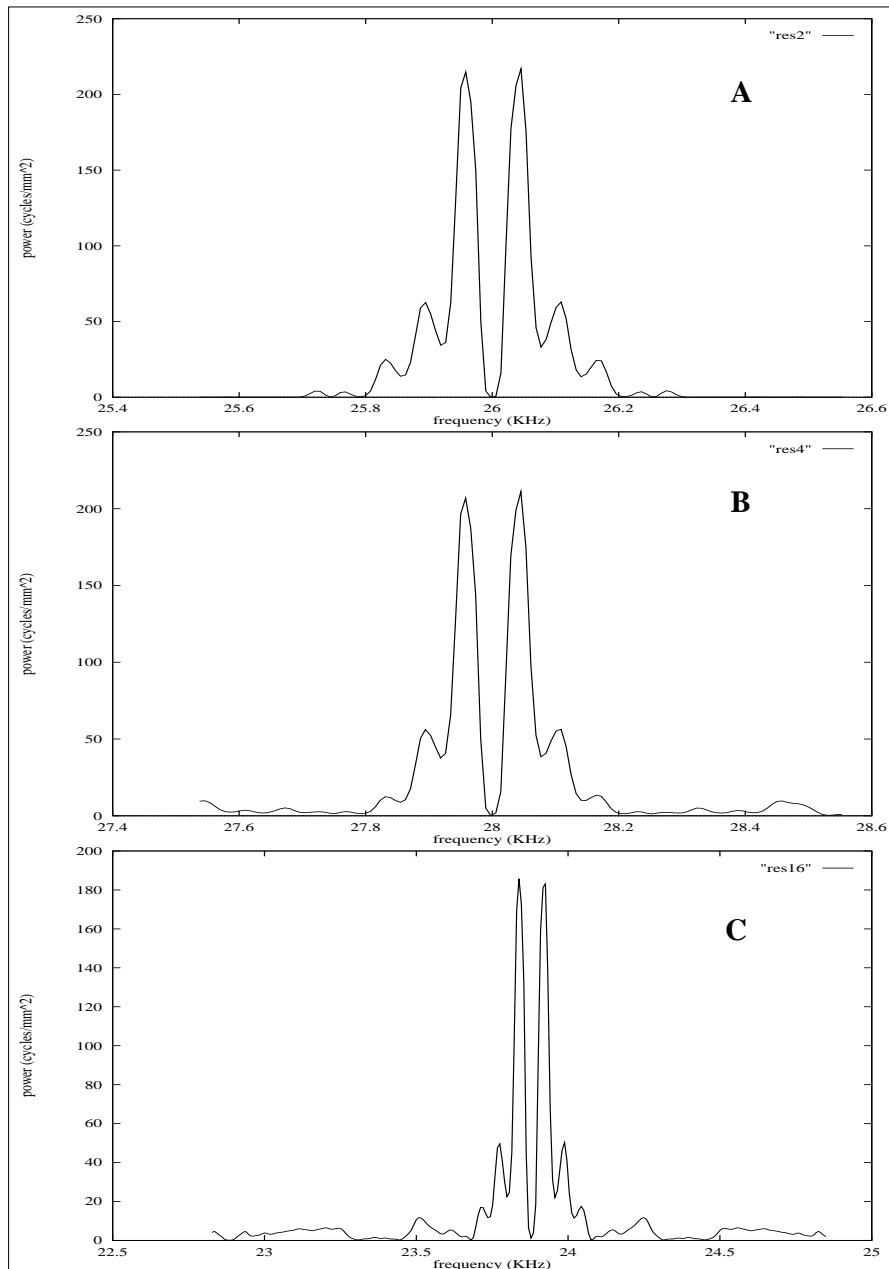
Figure 3: Periodogram analysis on simulated MR image data: (A) Power spectrum estimation of a static object. (B) Periodogram of a point-like moving object (frequency of motion 0.10 Hz). (C) As in (B) where ROPE is applied.

All the examples discussed below are the Lomb-Scargle periodogram windows around the highest observed power spectral density $P(f_{\max})$. These plots contain 256 periodogram points.
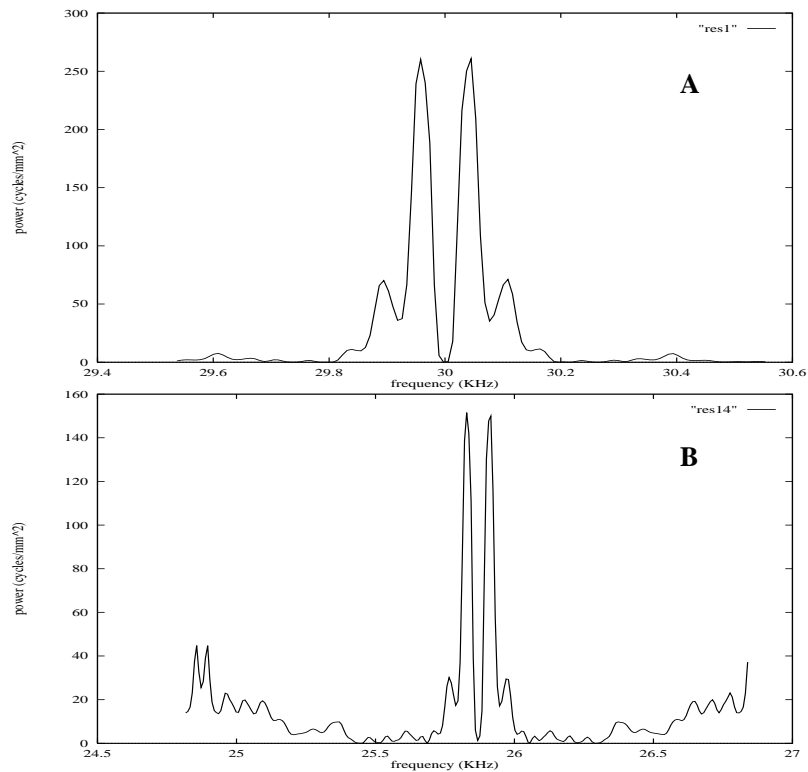
Figure 4: Periodogram analysis on simulated MR image data: (A) The Lomb-Scargle periodogram of a point-like moving object (frequency of motion 0.25 Hz). (B) As in (A) where ROPE is applied.

Figure 7 shows the comparison between the power spectra of the real (7.A) and imaginary (7.B) k-space data of a moving phantom's image. We clearly identify multiple periodic signal harmonics, away from the main peak of the power spectrum. In the case of the real data set, we can identify peaks at frequencies 1.75 Hz and 2.25 Hz. Their frequency shift from the next significant peaks (1.90 Hz and 2.10 Hz respectively) is a 0.15 Hz frequency difference. A similar and consistent observation can be made for the imaginary part of this data set. One can identify significant spectral peaks that have frequency differences of 0.15 Hz. For example, we can identify the following pairs: 4.75 Hz − 4.90 Hz, 4.82 Hz − 4.97 Hz, 5.03 Hz − 5.18 Hz and 5.10 Hz − 5.25 Hz. These frequency shifts strongly suggest the existence of the effect of the spurious motion artefact on the MR signals.

Figure 8 repeats the periodogram experiment for the case of the moving phantom image, corrected by the ROPE method. Here, the small peaks seen outside the central area of power spectral densities do not comply with the detection condition, and so they do not represent significant periodic signals. However, one can make some qualitative observations. The level of noise in the power spectrum has been reduced and the maximum observed power has been increased. The appearance of the periodograms indicate that ROPE tries to

16
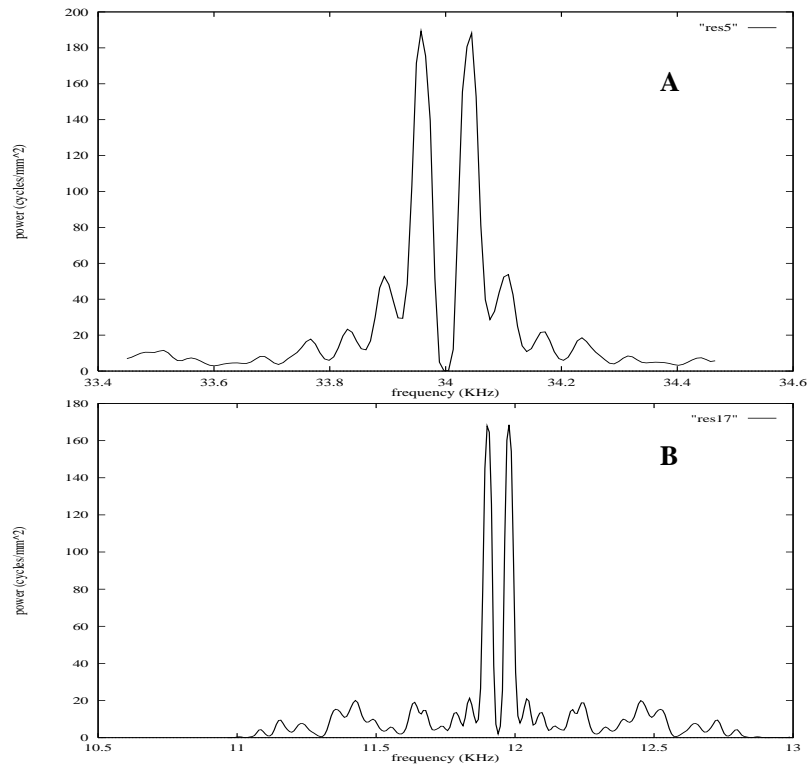
Figure 5: Periodogram analysis on simulated MR image data: (A) The Lomb-Scargle periodogram of a point-like moving object (frequency of motion 0.35 Hz). (B) As in (A) where ROPE is applied.

"put back" the artefact into the original signal. However, as seen in both real (8.A) and imaginary (8.B) parts of the data set, such lower harmonics exist within the area of the main signal, although a successful ROPE correction has been accomplished.

We have investigated the normalised Lomb-Scargle periodogram of data that has been acquired without the presence of the phase encoding gradient (see figure 9). It is clear that the effects seen in the two previous examples clearly disappear, a fact that indicates that the motion artefact appears mainly in the phase encoding direction of MR images.

Figures 10.A, 10.B and 10.C are the power spectral estimations for the real data sets of images with different resolutions. We have acquired images of the moving phantom for 16 × 32, 32 × 64 and 64 × 128 matrices. It is clearly seen that as the matrix size increases, the effect of the motion artefact becomes prominent. A similar effect can be observed on the imaginary part of the above data sets (see figure 11).

Finally, we investigated the appearance of the periodogram on an averaged image data set. Figure 12 shows the real and imaginary parts of k-space (plates A and B, respectively) of the moving phantom image. Here, each phase encoding step has been repeated four times and an averaged signal was acquired. On can

17
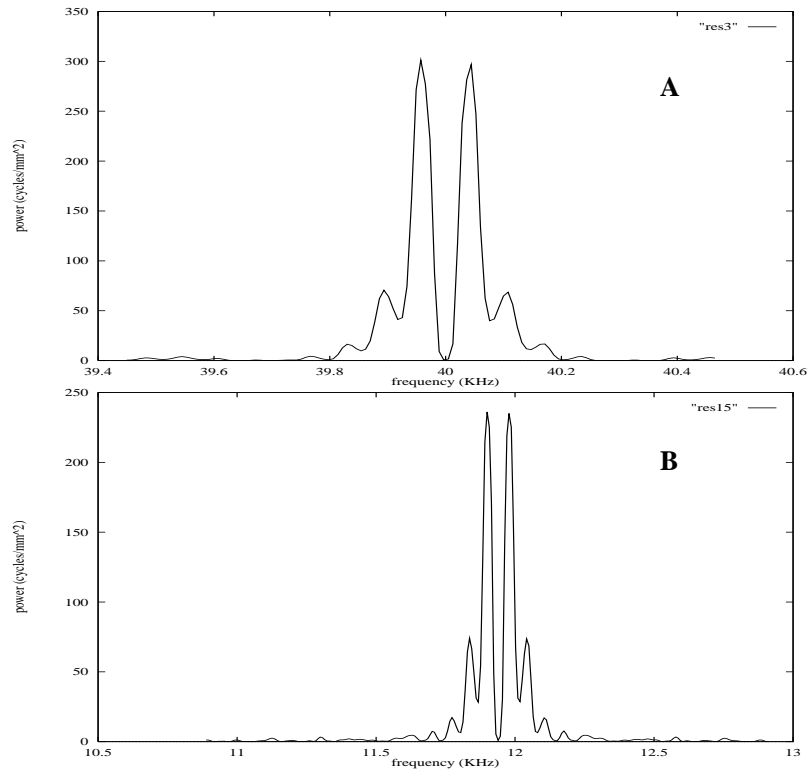
Figure 6: Periodogram analysis on simulated MR image data: (A) The Lomb-Scargle periodogram of a point-like moving object (frequency of motion 0.45 Hz). (B) As in (A) where ROPE is applied.

observe the lack of spurious harmonics outside the main are of the signal.

These results will be further discussed in section 6.2.

5.3   Periodogram Analysis on Experimental Spectroscopy Data

The most interesting application of the Lomb-Scargle periodogram has been found on the analysis of spectroscopic data. In a set of experiments, under the name *mot2* we have investigated the behaviour and appearance of the periodogram for the case of 1D CSI spectroscopic data. The size of the k-space matrices examined was 128×64. As in the case of 2D-FT imaging data, we formulated a single time series from the k-space data matrix points. The input time series data set consisted of 8,192 points. Again, for each point we assigned a corresponding observation time variable. The sampling of the MR signal was performed every 0.8 msec, while the TR was 1000 msec. The total experiment time per spectrum was 64 seconds.

The Lomb-Scargle periodogram has been evaluated at 16,384 independent frequencies, ranging from 0 kHz to the periodogram's experimental Nyquist frequency, which for this case was 64 kHz. The significance of the power spectrum
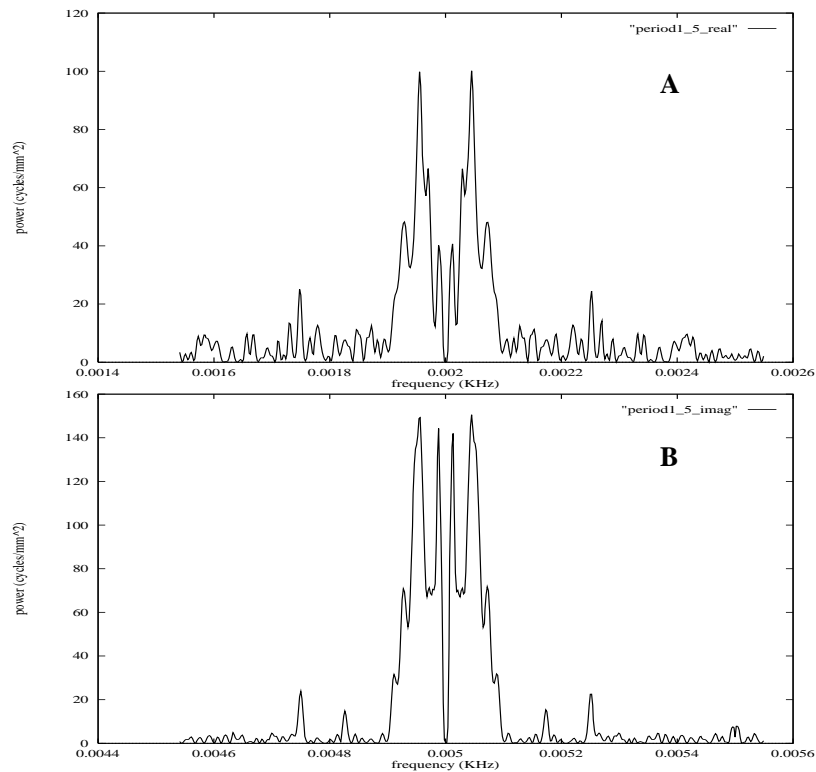
Figure 7: The normalized Lomb-Scargle periodogram of a moving phantom. Power spectral estimation on the real (A) and imaginary (B) parts of the k-space data.

levels has been again evaluated by using the false alarm probability condition that Scargle introduced (see equations 14, 15, and 16). For these experiments, we have again set a significance level of 95%, which determines a detection threshold $z_o = 12.7 \text{cycles}/\text{mm}^2$. So, below this threshold, any observed peak is classified as pure noise.

Figure 13 compares the periodograms of stationary (A), moving (B) and ROPE'd (C) phantom spectroscopic data. The periodogram is evaluated only for the real part of the signal. It is clear that figure 13.B shows additional harmonics, contaminating the pure signal. This suggests strongly that the effect of motion in MR spectra can be diagnosed by the Lomb-Scargle Periodogram. As we discussed in [6], motion effects are not easily detectable in spectra. Usually, one detects an increased noise level and consequently a loss in the expected signal to noise ratio. Frequently, due to this manifestation of the breathing artefact, spectroscopists do not suspect the existence of any systematic errors. These results suggest very strongly that this technique can become a valuable tool for MRS.

The visual observation of both the artefacted and ROPE'd spectroscopic data justifies our findings for the application of ROPE in spectroscopic CSI. Actually, the motion artefact is characterized in our experiments by three factors
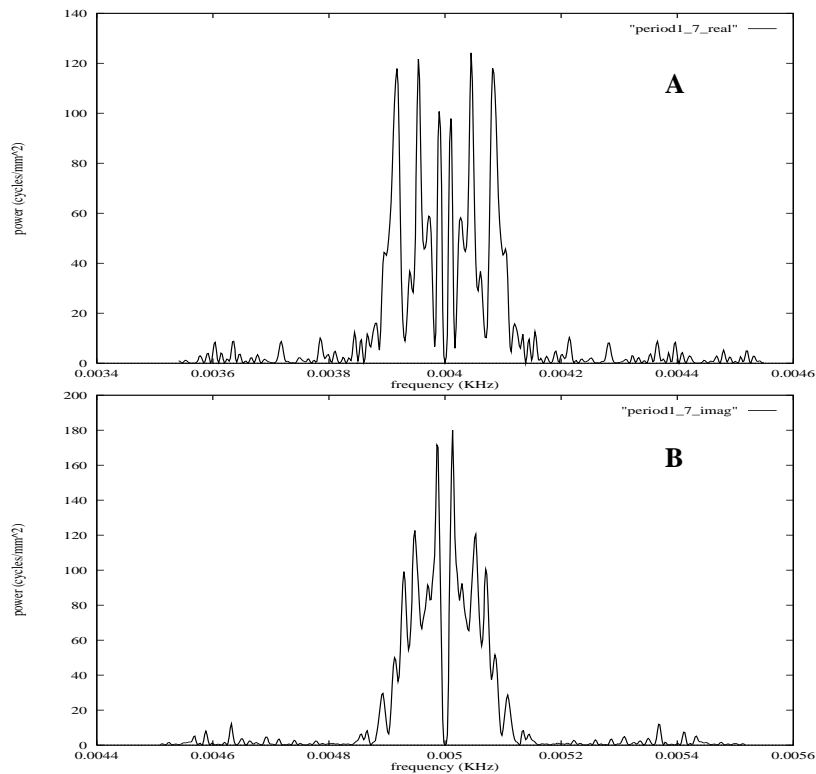
Figure 8: The normalized Lomb-Scargle periodogram of a moving phantom, treated with ROPE. Power spectral estimation on the real (A) and imaginary (B) parts of the k-space data.

in the periodogram:

- The existence of significant harmonics, additional to the main peak corresponding to the power of the signal.

- The reduced total power, observed on the maximum peak $P(f_{\max})$.

- The increased level of noise.

Unfortunately, it has proven very difficult to extract any quantitative data from these experimental results. This difficulty can be explained by the fact that MR data, unlike astronomical data for which the Lomb-Scargle Periodogram was originally intended, might present a more complex spectral composition, because of the way in which MR signals are acquired. The encoding processes in both MRI and MRS create rapid changes and variation on the spectral content of the observed signal. These variations might not allow the identification of consistent quantitative changes (related to the breathing artefact) in the periodogram.
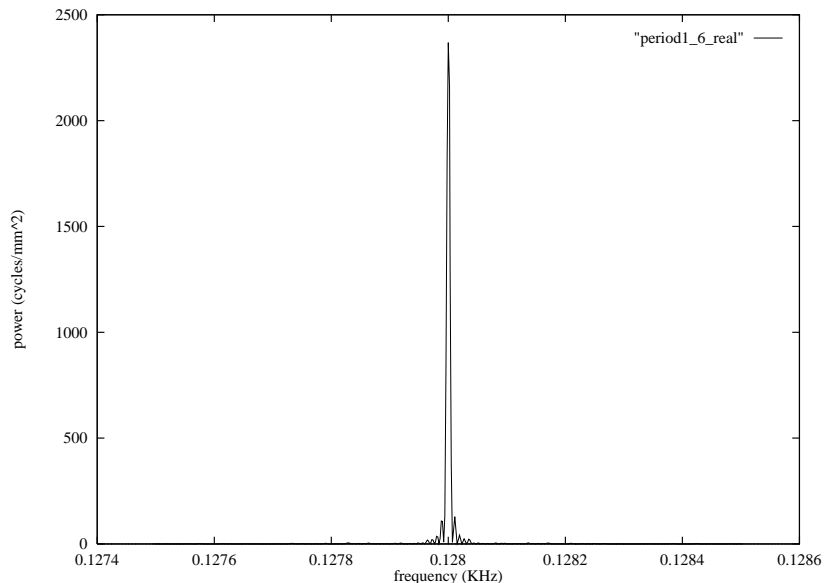
Figure 9: Example of an artefacted image data, acquired without the presence of the phase encoding gradient.

6 Discussion

6.1 The Application of the Lomb-Scargle Periodogram to Simulated MR data

The idea behind the use of simulated data to evaluate the output of the normalized Lomb-Scargle periodogram was to try to create time series data sets where we would have prior knowledge of the amplitude, period and pattern of the motion. We have attempted to identify both quantitative and qualitative factors for the characterization of motion artefacted data. We have concluded that the total spectral power from signals belonging to data sets contaminated by the effects of motion is usually observed to be reduced, if compared with "clean" images. It seems that the shape of the power spectral peaks is altered due to the effect of motion. Moving objects produce periodograms, which have a "rough" appearance if compared to the more "settled" appearance of static objects, as can be seen in figures 3.B, 4.A, 5.A and 6.A, where these periodograms have an increased level of noise, which in one of the cases (figure 5.A) appears as spurious harmonics, shifted from the pure signal.

One interesting aspect of these results was that the frequency at which the $P(f_{\max})$ is observed in a data set of a static object, is dramatically shifted as the frequency of motion increases. The application of the ROPE algorithm shows that this shift is re-instated in the appearance of the periodogram. However, one can easily identify the increased spurious effects that ROPE'd data produce on the normalized Lomb-Scargle periodogram. This can be explained by the fact that ROPE fails to reduce high-order ghosts and in some cases cannot eliminate the effects of blurring. In particular, this is shown on the power

21
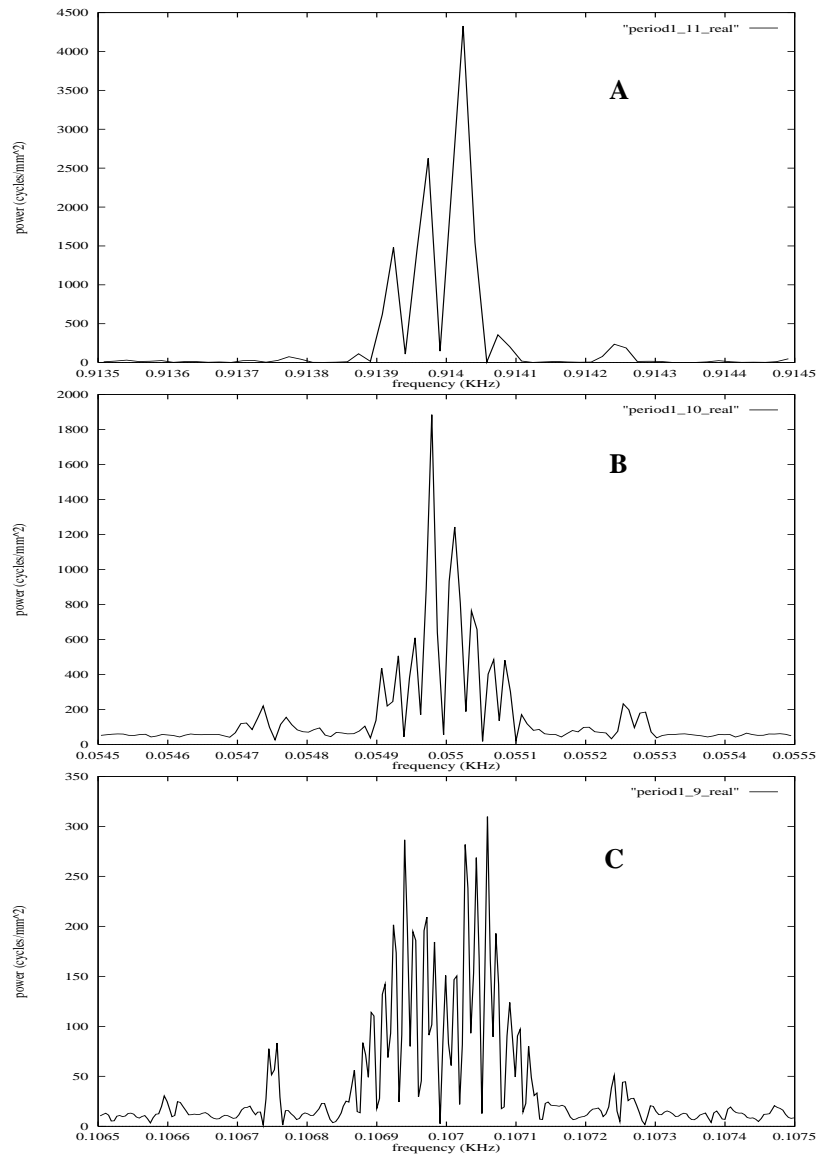
Figure 10: The Lomb-Scargle periodogram for image data (real part) with different matrix sizes: (A) 16 × 32, (B) 32 × 64 and (C) 64 × 128.

spectral estimation of a ROPE'd data set in figure 4.B.

All this knowledge we acquired from the simulated periodogram experiments is essential for the understanding of the appearance of the normalized Lomb-Scargle periodogram on experimental data. We discuss these results in the next section.
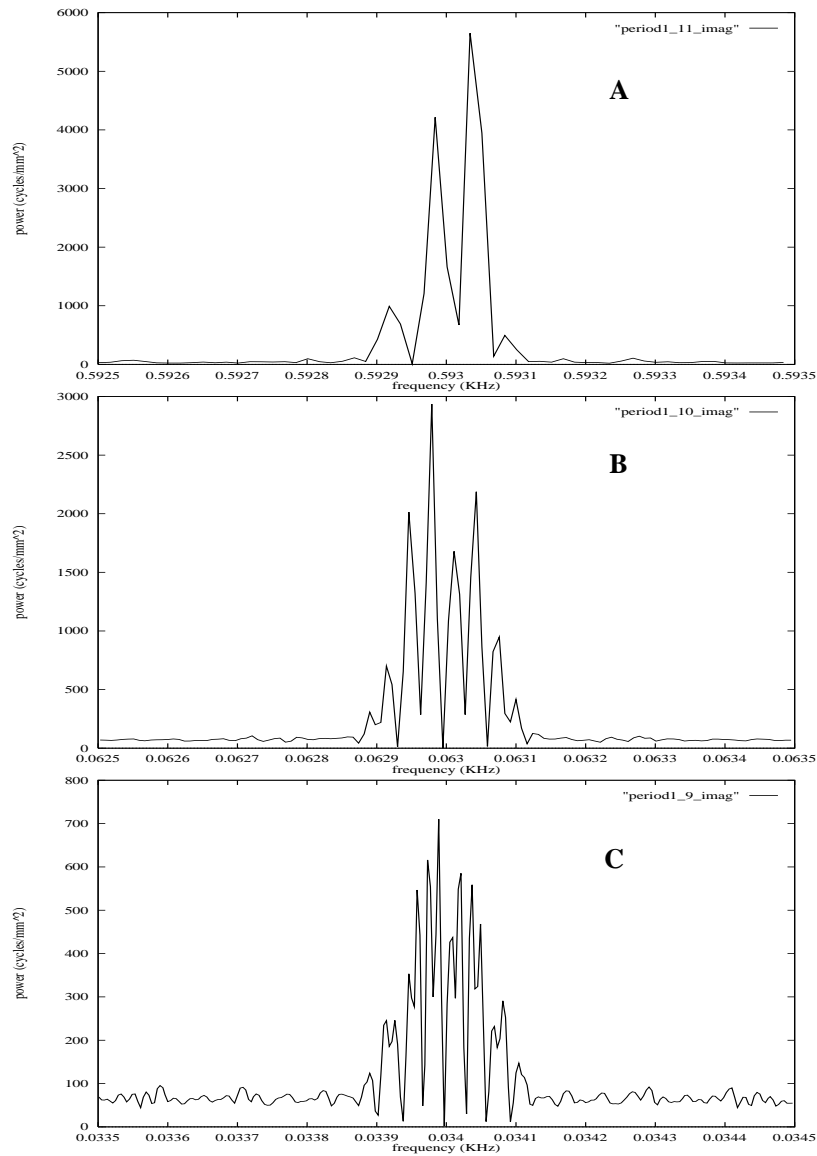
Figure 11: The Lomb-Scargle periodogram for image data (imaginary part) with different matrix sizes: (A) 16 × 32, (B) 32 × 64 and (C) 64 × 128.

6.2 Can the Lomb-Scargle Periodogram be a Valuable Tool for Analysis of Experimental MR data?

In this section of our discussion, we elaborate on the observations made on the application of the Lomb-Scargle periodogram on experimental MRI and MRS data.

In section 5.2 we examined the appearance of the periodogram on 2D-FT MRI data. As can be seen from all examples, the periodograms have a more
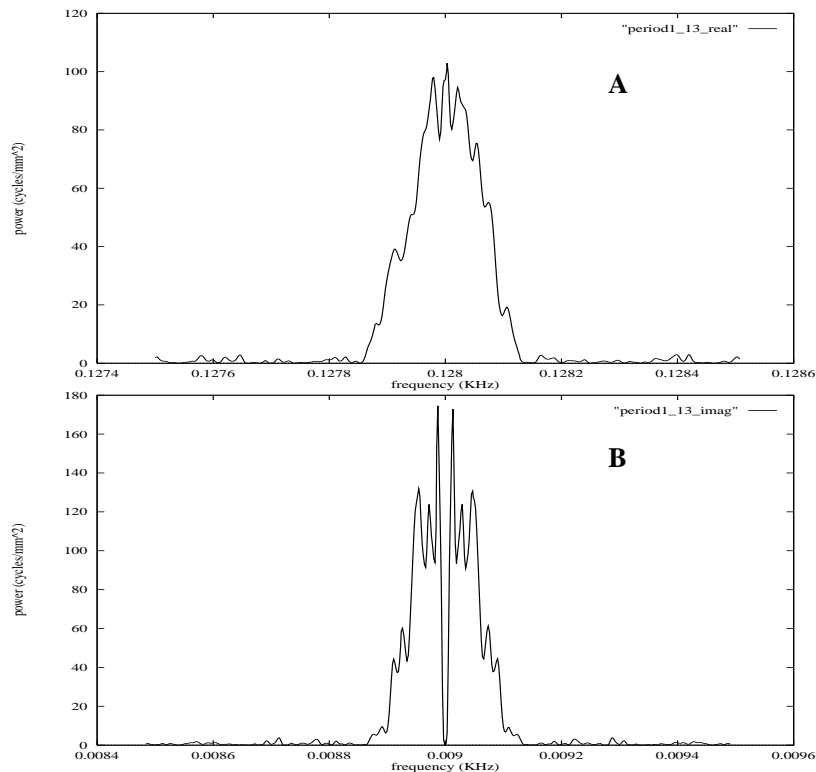
Figure 12: Signal averaging and the Lomb-Scargle periodogram.

complex structure. In figure 7 we showed a comparison between the power spectra of the real (7.A) and imaginary (7.B) k-space data of a moving phantom's image. We have clearly identified multiple periodic signal harmonics occurring at various distances from the main peak of the power spectrum. It was very interesting to discover, for both real and imaginary data, a consistent frequency shift between these harmonics and the main power spectral peaks. As we showed, this difference was equal to a 0.15 Hz[8] frequency difference. Although it is unclear how this quantity is related to the artefactual character of motion, it might be an indication to identify the frequency modulation that motion introduces to the MR signal. However, as the method of extirpolation of the fast periodogram algorithm arteficially creates an "even-like" sampling of the MR time series data, it might as well affect this sampling frequency value. Furthermore, spatial encoding (i.e. phase and frequency encoding) of the MR signal might affect the spectral content of the periodogram. Unfortunately, we cannot yet claim that the Lomb-Scargle periodogram gives us quantitative information for the study of MR data.

In figure 8 we repeated the periodogram experiment for the case of the moving phantom image, corrected by the ROPE method. Here, one can make qualitative observations. As in the case of the simulated data, the level of noise

---

[8] It is interesting to note that the motion frequency was also 0.15 Hz.

24
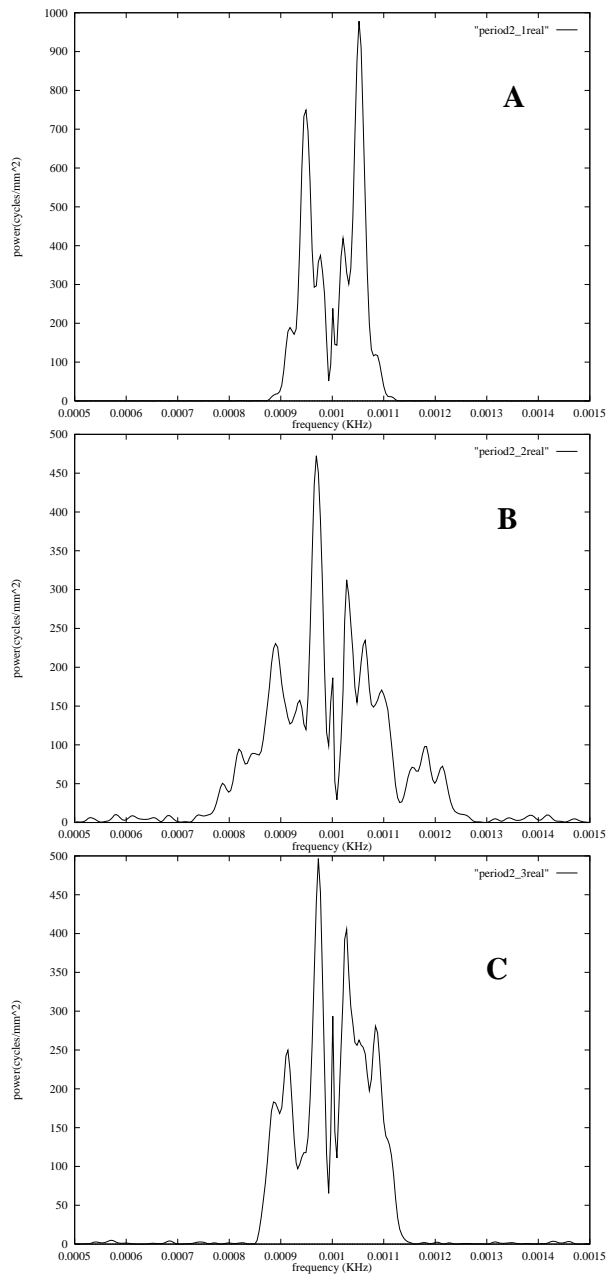
Figure 13: Lomb-Scargle periodogram analysis of spectroscopic data. (A) The power spectrum estimation for spectra measure on a stationary phantom and (B) on a moving phantom. (C) Periodogram of motion artefacted spectroscopic data that has been treated by the ROPE method.

in the power spectrum has been reduced and the maximum observed power has been increased. The appearance of the periodograms indicate that ROPE tries

to "put back" the artefact on the original signal. However, as seen in both real (8.A) and imaginary (8.B) parts of the data set, lower harmonics exist within the area of the main signal, although a successful ROPE correction has been accomplished. This again may correspond to the inability of ROPE to correct high-order ghosts and to deal with the effects of blurring.

The other observations made on the examples of data with different matrix size and averaged artefacted data are purely qualitative and prove once again some known factors that increase or reduce the intensity of the motion artefact. This result enhances our position that the Lomb-Scargle periodogram cannot be used as a quantitative tool for assessing k-space MR data. Moreover, this fact forbids the technique from being used as an indicator for the control of the motion artefact. However, the results found in the case of MR spectroscopic data are more promising. The visual observation of the periodogram of both the artefacted and ROPE'd spectroscopic data proves that the observed noise levels on spectra might originate from systematic errors as well. Our study showed that the motion artefact in MRS may be characterized by three factors in the Lomb-Scargle periodogram:

- The existence of significant harmonics, additional to the power of the signal.

- The reduced total power, observed on the maximum peak $P(f_{\mathrm{max}})$

- The increased level of random noise.

The above indicators, although at this stage qualitative, suggest that the Lomb-Scargle method could be more generally used as a diagnostic tool for identifying other systematic errors in human *in vivo* spectroscopic experiments.

7   Conclusion

Our study strongly suggests that the Lomb-Scargle periodogram can offer interesting qualitative information, relating to the effect of motion artefacts in both clinical MRS and MRI. Our observations, in particular for the case of MRS, lead us to the conclusion that the Lomb-Scargle periodogram could be more generally used as a diagnostic tool for identifying technical errors in human *in vivo* spectroscopic experiments. At present, the fast algorithm calculates the periodogram within a time span of four minutes, even for large data sets consisting of 65,536 points. Appropriate code optimization can improve the calculation time of the periodogram. Then, this technique can be used in real-time as a quick diagnostic method of the state of spectroscopic systems. If necessary, the MRS system can then be re-calibrated or an appropriate action to eliminate systematic errors can be taken.

We believe that through this paper we offer a new point of view in the study of the respiratory motion artefacts in MRI and MRS. Moreover, we have identified a new technical diagnostic tool that can be further developed and used to detect systematic errors in MR systems.

Acknowledgments

References

[1] T. W. Anderson. *The Statistical Analysis of Time Series*. Wiley, New York, 1971.

[2] T. N. Arvanitis. A model for magnetic resonance image formation. In C. Wood, R. Davidge, and P. Costa, editors, *The Fifth White House Papers, Graduate Research in Cognitive Sciences at Sussex, CSRP 251*, pages 1–3. School of Cognitive and Computing Sciences, University of Sussex, Brighton, 1992.

[3] T. N. Arvanitis. The two-dimensional Fourier Transform (2D-FT) imaging method in MRI: A computational approach. In J. K. Brook and T. N. Arvanitis, editors, *The Sixth White House Papers, Graduate Research in Cognitive Sciences at Sussex, CSRP 300*, pages 14–18. School of Cognitive and Computing Sciences, University of Sussex, Brighton, 1992.

[4] T. N. Arvanitis. *A Study of Respiratory Motion Artifacts in Magnetic Resonance Imaging and Spectroscopy*. DPhil thesis, University of Sussex, Brighton, UK, 1994.

[5] T. N. Arvanitis. Time-series analysis of MR data: Can the Lomb-Scargle periodogram be used in the future as a diagnostic tool for the identification of systematic errors in clinical MRI? In *On-line Proceedings, JMRM Internet Conference, The Future of Magnetic Resonance in Medicine*, Kyoto, Japan, 1997.

[6] T. N. Arvanitis, D. J. Bryant, A. G. Collins, G. A. Coutts, and A. S. Hall. An investigation of motion artefact in spectroscopic CSI. In *Proceedings of the 12th annual meeting of the SMRM*, page 909. Society for Magnetic Resonance in Medicine, August 1993.

[7] T. N. Arvanitis and D. Watson. Overcoming respiratory motion artifacts in MRI. In *Book of Abstracts, IEE Colloquium: Medical Imaging: Image Processing and Analysis*, pages 1–3, March 1992.

[8] T. N. Arvanitis and D. Watson. Computer modelling of the two-dimensional Fourier transform imaging method in MRI. In *Meeting Program and Abstracts, Royal Society of Medicine: Spring Meeting of the Forum on Computers in Medicine*, April 1993.

[9] T. N. Arvantis and D. Watson. Can the Lomb-Scargle periodogram identify systematic errors in MR data? *British Journal of Radiology*, 70(Suppl.):102, 1997.

[10] F. J. Beutler. Alias-free randomly timed sampling of stochastic processes. *IEEE Transactions of Information Theory*, 16:147–152, 1970.

[11] D. C. Black and J. D. Scargle. On the detection of other planetary systems by astrometric techniques. *The Astrophysical Journal*, 263:854–869, 1982.

[12] R. B. Blackman and J. W. Tuckey. *The Measurement of Power Spectra from the Point of Communications Engineering*. Dover, New York, 1958.

[13] P. Bloomfield. *Fourier Analysis of Time Series - An Introduction*. Wiley, New York, 1976.

[14] Ronald N. Bracewell. *The Fourier Transform and its Applications*. McGraw-Hill, New York, 1986.

[15] J. W. Brault and O. R. White. The analysis and restoration of astronomical data via fast Fourier transform. *Astronomy and Astrophysics*, 13:169–189, 1971.

[16] A. M. Breipohl. *Probabilistic Systems Analysis: An Introduction to Probabilistic Models, Decisions and Applications of Random Processes*. Wiley, New York, 1970.

[17] E. O. Brigham. *The Fast Fourier Transform and its Applications*. Signal Processing Series. Prentice-Hall, Engelwood Cliffs, NJ, 1988.

[18] D. C. Champeney. *Fourier Transforms and Their Physical Applications*. Academic Press, New York, 1973.

[19] C. Chatfield. *The Analysis of Time Series*. Chapman-Hall, London, fourth edition, 1989.

[20] D. G. Childers. *Modern Spectrum Analysis*. IEEE Press, New York, 1978.

[21] T. J. Deeming. Fourier analysis with unequally-spaced data. *Astrophysics and Space Science*, 361:137–158, 1975.

[22] W. Derbyshire. Standard phantoms for NMR imaging equipment. *Annali dell' Instituto Superiore di Sanita*, 19(1):163–7, 1983.

[23] D. F. Elliot and K. R. Rao. *Fast Transforms and Convolution Algorithms*. Academic Press, New York, 1982.

[24] A. L. Evans. *The Evaluation of Medical Images*. Adam Hilger Ltd., Bristol, 1991.

[25] D. J. Faulkner. Cepheid studies 1. more interaction in the beat Cepheid Utrianguli Australis. *The Astrophysics Journal*, 216:49–59, 1977.

[26] I. I. Gikhman and A. V. Skorokhod. *Introduction to the Theory of Random Processes*. Saunders, Philadelphia, 1969.

[27] Rafael C. Gonzalez and Richard E. Woods. *Digital Image Processing.* Addison-Wesley Publishing Company, Reading, Massachusetts, 1992.

[28] D. F. Gray and K. Deskachary. A new approach to periodogram analyses. *The Astrophysics Journal*, 181:523–530, 1973.

[29] D. M. Green and J. A. Swets. *Signal Detection Theory and Psychophysics.* Wiley, New York, 1966.

[30] E. J. Groth. Probability distributions related to power spectra. *The Astrophysical Journal Supplement Series*, 29(286):169–189, 1975.

[31] Joseph V. Hajnal, Ralph Myers, Angela Oatridge, Jane E. Schwieso, Ian R. Young, and Graeme M. Bydder. Artifacts due to stimulus correlated motion in functional imaging of the brain. *Magnetic Resonance in Medicine*, 31:283–291, 1994.

[32] J. C. Hancock and P. A. Wintz. *Signal Detection Theory.* McGraw-Hill, New York, 1966.

[33] J. R. Higgins. A sampling theorem for irregularly spaced sample points. *IEEE Transactions of Information Theory*, 22:621–622, 1976.

[34] J. H. Horne and S. L. Baliunas. A prescription for period analysis of unevenly sampled time series. *The Astrophysical Journal*, 302:757–763, 1986.

[35] G. M. Hyman and D. Booth. *Multivariate Time Series Analysis for Local Forecasting.* Number 11 in Occasional Papers. Centre for Environmental Studies, London, 1980.

[36] G. M. Jenkins and D. G. Watts. *Spectral Analysis and its Applications.* Holden-Day, San Francisco, 1968.

[37] Brian W. Kernighan and Dennis M. Ritchie. *The C Programming Language.* Prentice Hall, Englewood Cliffs, New Jersey, second edition, 1988.

[38] R. King. *Electrical Noise.* Chapman, London, 1966.

[39] N. R. Lomb. Least squares frequency analysis of unequally spaced data. *Astrophysics and Space Science*, 391:447–462, 1976.

[40] P. A. Lynn. *Digital Signals, Processors and Noise.* Macmillan, Basingstoke, 1992.

[41] D. D. Meisel. Fourier transforms of data sampled at unequal observational intervals. *The Astronomical Journal*, 83(5):538–545, 1978.

[42] D. D. Meisel. Fourier transforms of data sampled in unequal sized segments. *The Astronomical Journal*, 84(11):116–126, 1978.

[43] H. J. Nussbaumer. *Fast Fourier Transform and Convolution Algorithms.* Springer-Verlag, New York, 1982.

[44] A. V. Oppenheim and R. W. Schafer. *Discrete-Time Signal Processing.* Prentice-Hall, Engelwood Cliffs, NJ, 1989.

[45] A. Papoulis. *Signal Analysis*. McGraw Hill, New York, 1977.

[46] A. Papoulis. *Probability, Random Variables, and Stochastic Processed.* McGraw-Hill, New York, second edition, 1984.

[47] E. Parzen. *Stochastic Processes*. Holden-Day, San Francisco, 1962.

[48] E. Parzen. *Time Series Analysis Papers*. Holden-Day, San Francisco, 1976.

[49] W. H. Press and G. B. Rybicki. Fast algorithm for spectral analysis of unevenly sampled data. *The Astrophysical Journal*, 338:277–280, 1989.

[50] William H. Press, Saul A. Teukolsky, William T. Vetterling, and Brian P. Flannery. *Numerical Recipes in C: The Art of Scientific Computing*. Cambridge University Press, second edition, 1992.

[51] L. R. Rabiner and B. Gold. *Theory and Application of Digital Signal Processing*. Prentice-Hall, Englewood Cliffs, NJ, 1975.

[52] P. I. Richards. Computing reliable power spectra. *IEEE Spectrum*, 4(1):83–90, 1967.

[53] E. A. Robinson. *Time Series Analysis and Applications*. Goose Pond Publishing, Houston, Texas, 1981.

[54] J. D. Scargle. Studies in astronomical time series analysis II. Statistical aspects of spectral analysis of unevenly spaced data. *The Astrophysical Journal*, 263:835–853, 1982.

[55] M. Schwartz and L. Shaw. *Signal Processing: Discrete Spectral Analysis, Detection and Estimation*. McGraw-Hill, New York, 1975.

[56] H. L. Van Trees. *Detection, Estimation, and Modulation Theory: Radar-Sonar Signal Processing and Gaussian Signals in Noise*. Wiley, New York, 1971.

[57] J. W. Tuckey. *Spectral Analysis of Time Series*, pages 25–46. Wiley, New York, 1967.

[58] R. M. Weisskoff, J. Baker, J. Belliveau, T. L. Davis, K. K. Kwong, M. S. Cohen, and B. R. Rosen. Power spectrum analysis of functionally-weighted MR data: What's in the noise? In *Twelfth Scientific Meeting, Book of Proceedings*, volume 1, page 7. Society for Magnetic Resonance in Medicine, Berkeley, California, 1993.

[59] R. G. Wiley. Recovery of bandwidth signals from unequally spaced samples. *IEEE Transactions on Communications*, 26(1):135–137, 1978.

[60] Q. S. Xiang and R. M. Henkelman. Motion artifact reduction with three-point ghost phase cancellation. *Journal of Magnetic Resonance Imaging*, 1:633–642, 1991.